Effect of Headgroup Chirality in Nanoassemblies. Part 1. Self-Assembly of D-Isoascorbic Acid Derivatives in Water

Moira Ambrosi,[†] Pierandrea Lo Nostro,*[,†] Emiliano Fratini,[†] Luca Giustini,[†] Barry W. Ninham,[‡] and Piero Baglioni[†]

Department of Chemistry and CSGI, University of Florence, 50019 Sesto Fiorentino (Firenze), Italy and Department of Applied Mathematics, Research School of Physical Sciences and Engineering, Institute of Advanced Studies, Australian National University, Canberra, Australia 0200

Received: October 20, 2008; Revised Manuscript Received: December 01, 2008

L-(+)-Ascorbic acid and D-(−)-isoascorbic acid are epimers, with an opposite configuration at the C_5 stereogenic chiral center. Single-chained surfactants that carry a L-ascorbic or D-isoascorbic acid residue as hydrophilic headgroup and an alkanoate tail as hydrophobic chain were synthesized. We refer to these as L-ASC*n* and D-ASC*n*, with $n = 8$, 10, or 12. The role of the headgroup configuration in determining the nature of both the pure compounds and their nano assembly in aqueous dispersions were studied. Surface tension, infrared spectroscopy, differential scanning calorimetry, conductivity, small-angle X-ray scattering, and wide-angle X-ray diffractometry were used to characterize surfactant properties as a function of temperature and concentration. The L and D headgroup forms have significantly different hydration. This greatly affects the structure and stability of the aggregates in the micellar and coagel states.

Introduction

Vitamin C can be used as a versatile headgroup for the synthesis of surfactants.[1] These surfactants provide ideal candidates for exploring the effects of chirality on self-assembly. The headgroups possess two stereogenic centers, in positions 4 and 5 (see Figure 1), which generate four different epimers. Of these, L-(+)-ascorbic acid is the most familiar.

In previous papers we have investigated the properties of amphiphilic derivatives obtained via esterification of L-ascorbic acid in position 6 and of their nanoassemblies in aqueous dispersions.[2−6] In particular, depending on the chain length, 6-O-ascorbyl alkanoates (ASC*n*) produce micellar solutions (for $n = 8$ and 10) or gels (for $n \geq 11$). Longer chains ($n \geq 18$) form stable Langmuir monolayers at the air/water interface. On cooling, the ASC*n* form coagels in water. The coagels have a tight packing of the hydrocarbon chains.[7] The structures formed depend on concentration and hydrophobic tail length.

Although L-ascorbic acid is soluble essentially only in water, methanol, and ethanol,[8] the ASC*n* can also be dispersed in hydrophobic environments. There they act as excellent antioxidant agents, and they can be used to solubilize and protect lipophilic ingredients (drugs, vitamins, etc.) against radical attack.

D-(−)-Isoascorbic acid is an epimer of L-(+)-ascorbic acid (see Figure 1) with an inversion of the configuration at C_5. It is an active antioxidant agent.[9] However, it possesses only 1/20 of the biological activity of Vitamin C.[10] This is because the reducing and acidity properties of the ascorbic epimers are due to the furan ring, the enediol group, and the carbonyl in position 1, whereas the biological effect is related to the side chain.[11]

Chiral surfactants usually bear a sugar or an amino acid derivative as polar headgroup and are commonly studied for enantiomeric separations.[12] Important processes such as molecular recognition and self-organization, which are common in biomembranes and other biological supramolecular structures, are directly related to the chiral properties of the constituents.[13] Chirality has been recognized as one of the main factors that lead to the formation of supramolecular structures from multimolecular building blocks.[14,15] In a previous paper we showed that a bolaform surfactant that carries two L-ascorbic acid rings as polar headgroups forms monodisperse nanorods in water. It does so because of its architectural features. These are: the presence of chiral and quite bulky headgroups, the presence of several residues that are involved in intermolecular hydrogen bonding, and the relative flexibility of the hydrophobic tail.[16] These promising results prompted us to undertake a more detailed study of the effect of headgroup chirality on the self-assembly of ascorbic acid-based surfactants.

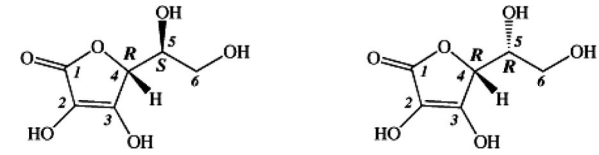

Figure 1. Molecular structures of L-ascorbic (left) and D-isoascorbic acid (right), showing the atomic numbering and the configuration of the chiral centers (C_4 and C_5).

We report a detailed study of aqueous dispersions of alkanoyl-6-O-D(−)-isoascorbic acid (D-ASC*n*). The results are compared to those obtained with alkanoyl-6-O-L-(+)-ascorbic acid (L-ASC*n*). The differences reflect effects due to the different chiral properties of the surfactant headgroup.

Materials and Methods

All reactants (analytical grade) were purchased from Fluka (Milan, Italy), and used without further purification. Bidistilled

* To whom correspondence should be addressed. Fax: +39 (055) 457-3036; e-mail: pln@csgi.unifi.it; website: http://www.csgi.unifi.it/.
[†] University of Florence.
[‡] Australian National University.

10.1021/jp8092644 CCC: $40.75
Published on Web 01/09/2009

water was purified with a MilliQ apparatus. NMR spectra were recorded with a Varian Jemini 300 spectrometer.

Synthesis. Octanoyl-, decanoyl-, and dodecanoyl-6-O-D-isoascorbic acid (D-ASC8, D-ASC10, and D-ASC12) were synthesized as described elsewhere.[1] The addition of a few drops of Br_2/CH_2Cl_2 to a solution of the D-isoascorbyl derivatives in acetone brings about instantaneous discoloration of bromine, confirming that the double bond of the headgroup is still active.

D-ASC8: yield 63.1%. The purity of the final product was assessed by TLC (eluent $CHCl_3/CH_3OH$, 4:1), which showed the presence of a single spot at $R_f = 0.70$. Elemental analysis was made after freeze-drying: Exptl: C, 54.70; H, 7.62; Calcd: ($C_{14}H_{22}O_7$ + 0.25 mol H_2O) C, 54.80; H, 7.39. IR (KBr disk) ν/cm^{-1} 3708−3000 (O−H), 2958, 2925, 2858 (C−H), 1764, 1744 (C═O ring), 1722 (C═O ester), 1705, 1686 (C═C), 1464, 1455 (CH_2 scissoring); NMR δ_H (300 MHz, DMSO; see Figure 1 for atom numbering) 0.89 (3H, CH_3−, t, $J = 6.3$ Hz), 1.28 (12H, 6 × CH_2−), 1.54 (2 × H_b, CH_2−), 2.32 (2 × H_a, CH_2−, t, $J = 7.2$ Hz), 4.08−4.03 (3H, 2 × H-6, H-5), 4.78 (H-4), 5.63 (OH, C_5−OH), 8.51 (OH, C_2−OH), 11.31 (OH, C_3−OH).

D-ASC10: yield 70.2%. The purity of the final product was assessed by TLC ($CHCl_3/CH_3OH$, 4:1), which showed the presence of a single spot at $R_f = 0.72$. Elemental analysis was made after freeze-drying: Exptl: C, 57.59; H, 8.23; Calcd: ($C_{16}H_{26}O_7$ + 0.2 mol H_2O) C, 57.54; H, 7.97. IR (KBr disk) ν/cm^{-1} 3733−2983 (O−H), 2950, 2917, 2850 (C−H), 1761, 1736 (C═O ring), 1708 (C═O ester), 1683, 1661 (C═C), 1469, 1455 (CH_2 scissoring); NMR δ_H (300 MHz, DMSO; see Figure 1 for atom numbering) 0.89 (3H, CH_3−, t, $J = 6.6$ Hz), 1.28 (12H, 6 × CH_2−), 1.54 (2 × H_b, CH_2−), 2.32 (2 × H_a, CH_2−, t, $J = 7.1$ Hz), 4.08−4.03 (3H, 2 × H-6, H-5), 4.78 (H-4), 5.62 (OH, C_5−OH), 8.50 (OH, C_2−OH), 11.30 (OH, C_3−OH).

D-ASC12: yield 76.4%. The purity of the final product was assessed by TLC ($CHCl_3/CH_3OH$, 4:1), which showed the presence of a single spot at $R_f = 0.72$. Elemental analysis was made after freeze-drying: Exptl: C, 60.41; H, 8.82; Calcd: ($C_{18}H_{30}O_7$) C, 60.32; H, 8.44. IR (KBr disk) ν/cm^{-1} 3692−3125 (O−H), 2951, 2914, 2847 (C−H), 1750, 1736 (C═O ring), 1711 (C═O ester), 1683, 1661 (C═C), 1469, 1455 (CH_2 scissoring); NMR δ_H (300 MHz, DMSO; see Figure 1 for atom numbering) 0.89 (3H, CH_3−, t, $J = 6.6$ Hz), 1.28 (12H, 6 × CH_2−), 1.53 (2 × H_b, CH_2−), 2.32 (2 × H_a, CH_2−, t, $J = 7.2$ Hz), 4.07−4.01 (3H, 2 × H-6, H-5), 4.78 (H-4), 5.60 (OH, C_5−OH), 8.49 (OH, C_2−OH), 11.26 (OH, C_3−OH).

Reducing Activity. The reducing activity (RA, %) was evaluated by measuring the absorbance at $\lambda = 517$ nm of a DPPH (α,α-diphenyl-β-picrylhydrazyl) solution in ethanol (10^{-4} mol/L) before (A_0) and after 20 min (A_{20}) from the addition of an equal volume of the sample (10^{-4} mol/L in ethanol or water). It is:[17]

$$\mathrm{RA}(\%) = 100\frac{A_0 - A_{20}}{A_0} \tag{1}$$

All derivatives possess a RA value larger than 95%. This is comparable to the typical values of L-ascorbic acid and its derivatives.[17]

Sample Preparation. The samples were prepared by weighing an appropriate amount of surfactant and water in a vial. To make sure that the delicate ascorbic acid ring remains intact, the samples were quickly annealed (four heating−cooling cycles around the phase transition temperature and storage in a refrigerator at 4 °C) in order to stabilize the sample and then immediately tested.

Surface Tension. Surface tension measurements on the D-ASC*n* solutions were carried out using a Du Noüy ring at 30 °C. The critical micellar concentration (cmc) was determined from plots of surface tension γ vs log c as the intersection point of the two measured straight lines for low and high concentrations. The surface tension (γ, in mN/m) vs log c plot for $c <$ cmc was used to calculate the polar headgroup area of the monomer (A_p, in Å^2/molecule), from the Gibbs equation for adsorbed monolayers at the air/water interface:[18]

$$\Gamma = -\frac{1}{2.303nRT}\left(\frac{\partial\gamma}{\partial \log c}\right) \tag{2}$$

$$A_p = (6.023\Gamma)^{-1} \tag{3}$$

where Γ, R, T, and N_A are, respectively, the surface excess of the surfactant, the gas constant (8.31 J/mol·K), the absolute temperature (K) and the Avogadro number. For nonionic surfactants $n = 1$, and for monovalent ionic amphiphiles $n = 2$.

The values of the volume (v_H) and the effective length (l_H) of the hydrocarbon tails in the fully stretched conformation were calculated after Tanford:[19]

$$v_H = 27.4 + 26.9(n - 1)$$

$$l_H = 1.5 + 1.265(n - 1)$$

pH Measurements. pH measurements were carried out at 20 °C with a Crison Basic 20 pH meter, equipped with a Crison glass electrode and an Ag/AgCl electrode as internal reference. The pH meter was calibrated with standard buffer solutions at pH 4.0, 7.0, and 9.0.

Conductivity. The critical micellar temperature (CMT) was determined with 10% w/w aqueous solutions by measuring the specific conductivity change of the ascorbyl-alkanoate dispersions as a function of temperature, using a radiometer type CDM conductimeter with a 1.25 cm^{-1} cell constant.

Medium-Infrared Spectroscopy. MIR spectra were acquired in the wavenumber interval 4000−650 cm^{-1}, with a Nexus 970-FTIR (Thermo-Nicolet) using KBr beam splitter and MCT/A detector, with a resolution of 8 cm^{-1} and coadding 64 scans.

Near-Infrared Spectroscopy. NIR spectra were acquired in the wavenumber range 8000−4000 cm^{-1}, with a Nexus 870-FTIR (Thermo-Nicolet) and a FT-IR Continuum microscope in diffuse reflectance mode (beam splitter: CaF_2; detector: MCT/A) with a resolution of 8 cm^{-1} and coadding 64 scans.

Differential Scanning Calorimetry. The CMT for D-ASC*n* coagels was obtained through DSC runs with a Q1000 differential scanning calorimeter (TA Instruments), using hermetic aluminum pans, sealed under nitrogen atmosphere. The coagel−micelle and coagel−gel phase transition temperatures were taken as the temperature of the endothermic peaks.[6] For each surfactant, samples of the pure solid and of its aqueous dispersions with concentration 5, 10, 20, 40, 60, and 90% w/w were prepared. Then, runs were made at the rate of 5 °C/min. For measurement of the frozen, strongly bound water, the samples were first cooled to −60 °C and then heated to 20 at 0.5 °C.

X-Ray Diffraction. XRD diffractograms were recorded by a powder Bruker D8 Advance diffractometer (BRUKER axs) using Bragg−Brentano geometry, $\lambda = 1.54$ Å (Cu Kα).

TABLE 1: Physico-chemical Properties of L-(+)-Ascorbic and D-(−)-Isoascorbic Acid[34]

	L-(+)-ascorbic acid	D-(−)-isoascorbic acid
MW (g/mol)	176.13	
mp (°C)	192.1°	169.5°
ΔH_m (kJ/mol)	43.54	40.86
water solubility (g/L)	333	100
pK_{a1}	3.36	3.29

Experiments were carried out in the range $1.5° \leq 2\theta \leq 40°$, with a step size of 0.04° and a time/step of 1 s, setting voltage and current at 40 kV and 30 mA, respectively.

Small- and Wide-Angle X-ray Scattering. SAXS measurements were carried out with a HECUS SWAX-camera (Kratky) equipped with a position-sensitive detector (OED 50M) containing 1024 channels of width 54 μm. Cu Kα radiation of wavelength $\lambda = 1.542$ Å was provided by a Seifert ID-3003 X-ray generator (sealed-tube type), operating at a maximum power of 2 kW. A 10 μm thick nickel filter was used to remove the Cu K_β radiation. The sample-to-detector distance was 273 mm. The volume between the sample and the detector was kept under vacuum during the measurements to minimize scattering from the air. The Kratky camera was calibrated in the small angle region using silver behenate ($d = 58.48$ Å)[20] and lupolen ($d = 4.12$ Å) was used as reference materials for the wide-angle region. Scattering curves were obtained in the Q-range between 0.01 and 0.54 Å^{-1}, Q being the scattering vector $Q = (4\pi \sin\theta)/\lambda$, and θ the scattering angle. The covered WAXD region spans from 18 to 26° in 2θ. Solid samples were placed into 1 mm demountable cells having Kapton films as windows. Liquid samples were filled into a 1 mm quartz capillary. The temperature was controlled by a Peltier element, with an accuracy of ±0.1 °C. All scattering curves were corrected for the solvent and the empty cell contribution considering the relative transmission factor. SAXS curves from liquid samples were iteratively desmeared using the procedure reported by Lake.[21]

Results and Discussion

Solid State. ***Structural Features.*** The molecular structures of the parent acids, L-(+)-ascorbic acid and D-(−)-isoascorbic acid, are shown in Figure 1. These are epimers, as the configuration of the stereogenic center in position 5 is inverted but that of the carbon in position 4 is retained. The main physicochemical properties of the two acids are quite different, as shown in Table 1.

In particular, the melting point, the melting enthalpy change, the water solubility, and the first ionization constant pK_{a1} of D-isoascorbic acid are lower than those of L-ascorbic acid.

A careful perusal of the inter- and intramolecular interactions in the two acids suggests a plausible explanation for these different properties. Figure 2 shows some inter- and intramolecular hydrogen bondings (red dashed arrows). These involve the hydroxyl residue in position 2 and the carbonyl group in position 1 (Figure 2a) or 3 (Figure 2b). Figure 2c shows the intermolecular hydrogen bonding that involves the carbonyl in C_1 and the C_6−OH.[22] All these interactions can be present in both L-ascorbic and D-isoascorbic acids. On the other hand, an intramolecular hydrogen bond between the hydroxyl group in position 5 with the acidic −OH residue in position 3 can be formed only in D-isoascorbic acid (see Figure 2d and 2e). In the L-epimer such interaction is not favored, since the hydrogen in 4 points in the same direction as C_5−OH.

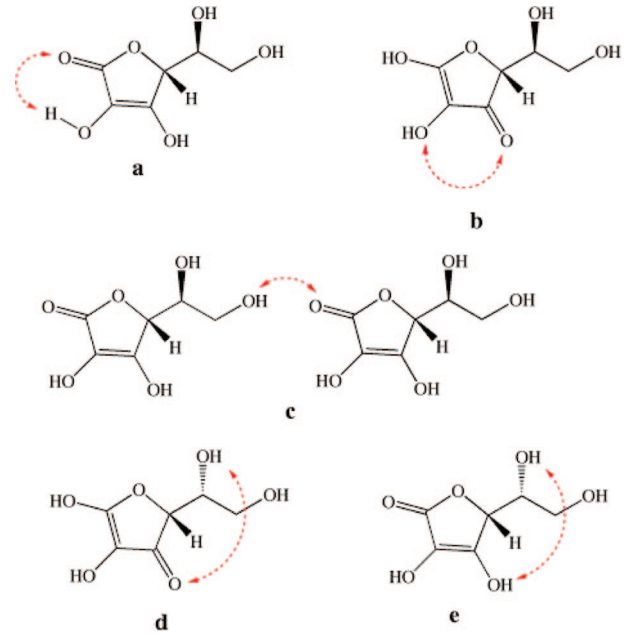

Figure 2. Some intra- and intermolecular interactions in L-ascorbic acid (a, b, c) and in D-isoascorbic acid (d, e).

Such differences in configuration and hydrogen bonding distribution result in a different behavior of the two epimers, particularly in their capacity to interact with like molecules in the pure solid and with water molecules in the dispersed state. Thus L-ascorbic acid is three times more soluble and a little less acidic than D-isoascorbic acid.[23] We remark that of the two −OH residues in the ring, that in position 3 is by far the most acidic. The acidity difference between L and D can be justified by considering that a more acidic C_3−OH donor group will strengthen the intramolecular hydrogen bonding with C_5−OH (see Figure 2). Furthermore, the intermolecular interactions between D-isoascorbic acid molecules in the condensed state are expected to be weaker than those in L-ascorbic acid, as the lower melting point and melting enthalpy change indicate.

The structure of L-ascorbic and D-isoascorbic acids have been fully characterized and reported in the literature. The most significant features are:

(i) In the crystal lattice of L-ascorbic acid, the unit cell contains two kinds of molecules, "A" and "B", that differ in the positions of hydrogen bound to the oxygen in 5 and 6.[24] Each molecule establishes eight intermolecular hydrogen bonds with vicinal molecules. No intramolecular hydrogen bond is present.[25−27] All oxygens participate in the formation of intermolecular hydrogen bonds, except the ether O atom in the lactone ring. The oxygens in 2, 5, and 6 act both as donor and acceptor, that in 3 as a donor, and that in 1 only as an acceptor.[25]

(ii) The similarity in the preferred conformations in the crystal and in solution for L-ascorbic acid seems to confirm the lack of intramolecular hydrogen bonding in this molecule. On the other hand, a well-defined hydration shell through intermolecular hydrogen bonding with the solvent is expected to occur.[28]

(iii) In the two epimeric acids the bond distances and angles of the atoms of the ring and of C_2OH and C_3OH do not vary markedly, but the angles of the −C_5HOH−C_6H_2OH side chain do differ significantly. This may also affect their ionization capacity.[29]

(iv) Concerning the interactions of the two epimers with the solvent, it has been suggested that L-ascorbic acid does not modify the dynamical structure of bulk water significantly,[28,30−33]

TABLE 2: Length (l_H, in Å) and Volume (v_H, in Å^3) of the Alkyl Chain in the Fully Stretched Conformation Calculated According to Tanford[19] and Spacings (d, in Å) for D-ASCn and L-ASCn Solids as Obtained from XRD Experiments

			d			
			D-ASCn		L-ASCn	
n	l_H	v_H	hydrated	anhydrous	hydrated	anhydrous
8	10.3	216	30.5	21.9	31.7	
10	12.9	269	34.2	24.5	34.5	22.6
12	15.4	323	37.2	28.0	38.7	

whereas D-isoascorbic acid has a strong impact on the bulk solvent. On the other hand, the amount of hydrated water is larger for L-ascorbic than for D-isoascorbic acid presumably because in the latter case intramolecular interactions reduce the number of sites available for hydrogen bonding with the water molecules.

Given such premises, we performed IR, XRD, and DSC experiments to study the behavior of the two epimeric acids and of their derivatives in the solid state.

Infrared Spectroscopy. The NIR spectra were acquired for L-ascorbic and D-isoascorbic acid between 8000 and 4000 cm^{-1}, and are shown in Figure S1a (see Supporting Information). Different peaks appear in the two cases, especially between 7000 and 5000 cm^{-1} (see Figures S1b and S1c, Supporting Information), and in the 4500−4000 cm^{-1} region. The former is due mainly to the first overtone stretching for OH groups. The latter corresponds to a combination of C═O, O−H, and C−H stretching.[22] The differences between the two epimeric acids appear as shifts to lower or higher wave numbers. For example, the peak at 6721 cm^{-1} for L-ascorbic acid is assigned to an OH first overtone stretching vibration involved in an intramolecular hydrogen bonding (Figure 2a).[35] It shifts to 6738 cm^{-1} for D-isoascorbic acid and is much more intense.

More significantly, the peak at 7837 cm^{-1} for L-ascorbic acid, assigned to the first overtone asymmetric stretching for an intermolecular hydrogen bonding,[22] has disappeared in the NIR profile of D-isoascorbic acid (see Figure S1c, Supporting Information).

Figures S2 and S3 (Supporting Information) show the MIR spectra of L-ascorbic acid, D-isoascorbic acid, and their ester derivatives, in the ranges 3750−2000 and 1800−1600 cm^{-1}, respectively. L-ascorbic acid shows four intense peaks that correspond to the intermolecularly hydrogen bonded O−H residues in positions 6 (3526 and 3315 cm^{-1}) and 5 (3410 and 3215 cm^{-1}). At lower wave numbers, between 3100 and 2200 cm^{-1}, a set of broad bands and sharp peaks appears, due to the O−H groups in positions 2 and 3 and to the C−H stretching, respectively. D-Isoascorbic acid shows two sharp peaks due to the stretching of the O−H groups in position 6 (3484 cm^{-1}) and 5 (3335 cm^{-1}). These are hydrogen bonded intramolecularly, and therefore shifted to lower frequency.[36−38] The broad bands between 3100 and 2200 cm^{-1} also appear for the D-epimer.

Regarding the derivatives, the MIR spectrum at high wavenumber changes in a consistent way, as the C_6−O− group is now involved in the ester bond. All L-ASCn show a sharp peak centered at 3396 cm^{-1}, due to the stretching of the C_3O−H or C_5O−H, and a smaller and broad band between 3300 and 3160 cm^{-1}. Presumably that is related to the presence of some water of hydration. In the range between 3000 and 2800 cm^{-1} new sharp peaks appear, due to the side alkyl chain.

The D-ASCn derivatives show a strong peak at 3410 cm^{-1} (stretching of the C_3O−H or C_5O−H), a broad band between 3300 and 3000 cm^{-1}, less significant than that for the L-ASCn, and signals due to the alkyl chains.

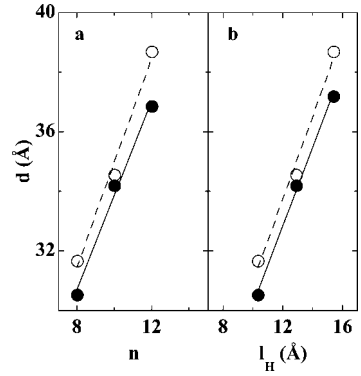

Figure 3. Variation of the lamellar spacing (d) for L-ASCn (○) and D-ASCn (●), as a function of the number of carbons in the hydrophobic chain (a) and of the tail length l_H (b).

At lower wavenumber the spectra show a band due to the C═O bond in the lactone ring (1754 cm^{-1} for L-ascorbic acid and 1761 cm^{-1} for D-isoascorbic acid) that shifts significantly for the ASCn derivatives, and the intense doublet between 1675 and 1660 cm^{-1}, due to the C═C stretching mode of the enediol group, is coupled with the neighboring vibrations of the conjugated system. For the D- and L-ASCn molecules this region of the spectrum is more complicated, presumably because of the different stabilization of the tautomers.

More bands appear in the fingerprint region: between 1327 and 1316 cm^{-1} for the C_2−OH deformation, at 1275 cm^{-1} for the C_2−O stretching, around 1140 cm^{-1} for C_5−O stretching, and between 1030 and 940 cm^{-1} for the deformations of the lactone ring.[36] In summary, MIR and NIR spectra confirm that in the two epimers there is a different set of inter- and intramolecular hydrogen bonding that is strictly related to the configuration at C_5.

X-ray Diffractometry. The structural properties of the pure solids were investigated through XRD experiments. Figure S4 (Supporting Information) reports that XRD profiles for L-ASCn and D-ASCn. Table 2 summarizes the spacings (d) calculated with the Bragg equation $d = n\lambda/(2 \sin \theta)$ for the lowest angle peak. All spectra show a strong sharp peak at low 2θ and other peaks at higher angles (>10°) due to chain packing.

In the intermediate region (4°−10°), peaks due to higher order reflections of a lamellar lattice are visible in spectra of derivatives with n ≥ 10. D-ASC8 and L-ASC8 possess less crystalline structure so that lamellar reflections are not present. Extra peaks in the low angle region, marked with an asterisk, are due to the anhydrous crystal. As expected, peaks due to anhydrous solids are more prominent for D-ASCn derivatives, which are less hygroscopic.

The lamellar spacings are plotted as a function of the number of carbons in the alkyl chain (n), in Figure 3a, and as a function of the hydrophobic tail length in its fully stretched conformation (l_H), in Figure 3b.

In both cases, d changes linearly with n and l_H. The slope $\partial d/\partial n$ is 1.6 ± 0.1 for D-ASCn and 1.7 ± 0.1 for L-ASCn, and the intercept for $n = 0$ is $d_0 = 19 \pm 1$ for D-ASCn and L-ASCn. The slope $\partial d/\partial l_H$ is 1.3 ± 0.1 for D-ASCn and 1.4 ± 0.1 for L-ASCn. All these values are consistent with an orthogonal monolayer phase,[39] with the surfactant molecules arranged in interdigitated, nontilted, and closely packed lamella. From the XRD spacings (d) and the length of the alkyl chains in the fully stretched conformation (l_H), we calculated that the thickness of

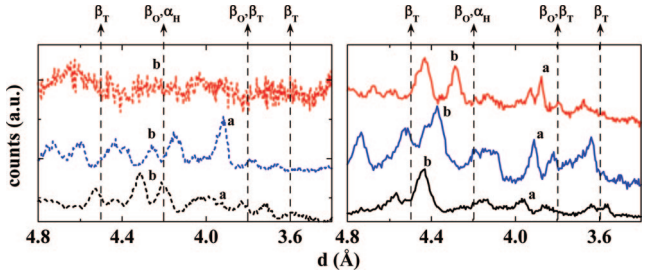

Figure 4. WAXD profiles between 4.8 and 3.4 for L-ASC*n* (dotted lines, left) and D-ASC*n* (full lines, right). Red: ASC8, blue: ASC10, black: ASC12. The vertical lines indicate the typical peaks for the α_H (4.2 Å), β_T (4.5, 3.8, and 3.6 Å), and β_O (4.2 and 3.8 Å) crystalline phases.

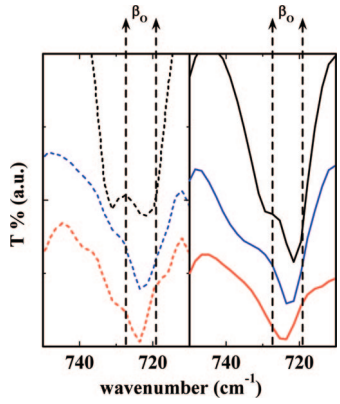

Figure 5. FTIR spectra between 750 and 710 cm^{-1} for L-ASC*n* (dotted lines, left) and D-ASC*n* (full lines, right). Red: ASC8, blue: ASC10, black: ASC12. The vertical lines indicate the absorption bands for the β_O (719 and 727 cm^{-1}) crystalline phase.[40]

the hydrophilic shell, $(d - l_H)/2$, is about 10−11 Å, in agreement with our previous findings.[2] If we repeat the same calculation using the *d*-spacing of the D-ASC*n* anhydrous phases, the length of the single headgroup drops down to a dramatically different 5−6 Å.

The crystal structure of the alkyl chains can be detected by looking more closely at the WAXD and FTIR profiles. Long chain alkanes can form different crystalline phases: hexagonal (α_H), orthorhombic (β_O), triclinic (β_T), and monoclinic (β_M), that produce specific peaks between 3 and 5 Å in WAXD spectra, and typical bands between 750 and 710 cm^{-1} in FTIR spectra.[40] Figures 4 and 5 show the presence of peaks at about 3.8 ("a") and 4.2 Å ("b") in the WAXD profiles, and of a dual absorption between 719 and 731 cm^{-1} in the FTIR spectra that suggest the presence of the β_O structure as the main crystalline phase.[41]

Differential Scanning Calorimetry. DSC runs were performed on the pure solid D-ASC*n* compounds to determine the melting point (T_f), the enthalpy change of melting (ΔH_m), and the entropy change of melting ($\Delta S_m = \Delta H_m/T_f$). The data for D-ASC*n* are listed in Table 3 and are plotted in Figure S5 (Supporting Information). For all derivatives, T_f, ΔH_m, and ΔS_m increase as a function of the hydrophobic chain length. The D-isomers possess lower melting points but higher enthalpy and entropy changes of melting with respect to the L-isomers with the same chain. These values reflect the different intermolecular interactions in the pure solids, as will be discussed later.

Aqueous Dispersions. Once dispersed in water, at low temperature all of the ascorbyl alkanoates form coagels, that is, hydrated semicrystalline nanoassemblies separated from the water solution phase. Upon heating, these supramolecular

TABLE 3: Physico-Chemical Properties of L-ASC*n* and D-ASC*n*[a]

	ASC8		ASC10		ASC12	
	L	**D**	**L**	**D**	**L**	**D**
T_f (°C)	91.9	39.5	100.6	50.8	106.9	65.3
ΔH_m (kJ/mol)	15.68	18.03	25.67	32.60	39.21	41.15
ΔS_m (J/mol·K)	42.97	57.70	68.70	100.65	103.22	121.64
pH (1 mM)[b]	3.15	3.13	3.36	3.43	3.52	3.93
cmc (mM)[b]	1.060	5.380	0.344	1.410	0.033	0.123
cmc (mM)[c]	6.10	4.72	0.77	3.19	0.03	1.68
CMT (°C)[c]	19.3	22.9	36.8	32.7	44.5	44.9
A_p (Å²/molecule)[b]	48.9	46.5	47.0	45.0	46.8	38.8
p	0.42	0.45	0.44	0.46	0.45	0.54

[a] Melting Point (T_f), enthalpy change of melting (ΔH_m), entropy change of melting (ΔS_m), pH of a 1 mM solution in water, critical micellar concentration, critical micellar temperature (CMT), cross-section area per polar group (A_p, in Å²/molecule), and packing parameter (*p*). [b] From surface tension measurements. [c] From conductivity measurements at 30 °C for D-ASC8, 45 °C for D-ASC10, and 55 °C for D-ASC12.

structures produce either micellar solutions or viscous gels, depending on the side chain length. Figure S6 (Supporting Information) depicts the structure of the coagel, where the lamellar layers are separated by an extremely small interlayer of strongly bound water molecules. By contrast, in the gel phase instead, the hydrophobic tails rearrange and the aqueous pool contains additional "intermediate" water.[42]

The pH of 1 mM aqueous solution of L-ascorbic acid, D-isoascorbic acid, and their amphiphilic derivatives were measured at 20 °C. As expected, D-isoascorbic acid (pH = 3.30) is a little more acidic than L-ascorbic acid (pH = 3.32). Moreover, 1 mM solutions of L-ASC8 and D-ASC8 have the same pH, whereas the pH of longer surfactants is greater. The D-ASC*n* are less acidic than L-ASC*n* for $n = 10$ and 12. It is well-known that for fatty acids the ionization constant pK_a increases with the chain length, due to the formation of strong ion−dipole interactions between $RCOO^-$ and RCOOH species. These stabilize the charge and disfavor the deprotonation of more carboxyl groups in the aggregate (cooperativity).[43] A similar mechanism can be proposed for the ascorbyl headgroups, with a significant interaction between the ionized C_3-O^- residue and one of the hydroxyls of the adjacent molecule at the aggregate interface. The increment in pK_a is more significant as the chain length increases, because of the stronger van der Waals attractive interactions between the closely packed aliphatic chains.[43] In our case, 1 mM solutions of L-ASC8 and D-ASC8 are below the cmc (see Table 3). Therefore, the surfactants are in the monomeric state. Interestingly, the longer chained surfactants have a greater value of pK_a, and the D-ASC*n* surfactants are less acidic than L-ASC*n*. This finding is presumably due to the smaller area per polar headgroup for D-ASC*n*, which keeps the monomers closer to the micellar interface, and therefore disfavors the further ionization of adjacent headgroups.

At very low concentrations, ASC*n* form adsorption monolayers at the air−water interface. The critical micellar concentration (cmc) and the critical micellar temperature (CMT) of D-ASC*n* in water were determined through conductivity and surface tension measurements. The self-assembly behavior of these amphiphiles reproduces that of the L-isomers.

Figures S7 and S8 (Supporting Information) show the conductivity of D-ASC8 and D-ASC10 as a function of the surfactant concentration and as a function of temperature at [D-ASC*n*] = 10% w/w, respectively. The values of cmc and CMT were extracted from the plots[6] and are listed in Table 3.

TABLE 4: Structural Parameters Extracted from the Fitting of the SAXS Profiles for L-ASC8 and D-ASC8[a]

	L-ASC8	D-ASC8
R (Å)	9.0 ± 1	9.3 ± 1
τ (Å)	10.2 ± 1	9.6 ± 1
A_p (Å^2)	48	46
polydispersity	0.18	0.16

[a] See Figure S10, Supporting Information. Radius of the hydrophobic core (R), hydrophilic shell thickness (τ), area per polar head group (A_p), and polydispersity.

The data shown in Table 3 confirm that the CMT depends on the length of the aliphatic chain and does not vary significantly with the headgroup.[6] This suggests that it is the conformational and packing state of the hydrophobic segment that determines the phase transition. Figure S9 (Supporting Information) shows the surface tension of aqueous solutions of the surfactants as a function of log c at 30 °C. From the intersection point of the two fitting lines for high and low concentrations we determined the cmc (see Table 3). The cmc decreases with the length of the hydrophobic chain. The cmc for the D-ASCn molecules is almost five times that of the corresponding L-ASCn.

Compared to the cmc values obtained from conductivity measurements, the results are in good agreement, except for ASC12, because of the large difference in the experimental temperature.

From the slope of the γ/log c plot we calculated the area per polar group (A_p) from equations 2 and 3, and the values are reported in Table 3. The A_p values for the D-ASCn amphiphiles are always lower than those for the corresponding L-epimers, again presumably a result of the different hydration and ionization capacity of the polar heads.[29] This finding may explain the pH difference recorded for ASC10 and ASC12 discussed above.

Small-Angle X-ray Scattering. SAXS experiments were carried out on L-ASC8 and D-ASC8 aqueous micellar dispersions (5% w/w) at 20 °C. The spectra are shown in Figure S10 (Supporting Information). The data can be fitted using a log-normal distribution of a circular cylinder with a core−shell scattering length density profile,[44] according to the IGOR Pro package developed at the NIST Center for Neutron Research (NCNR).[45] As a first approximation, the shell thickness on the flat ends of the cylinder has not been taken into account, and the polydispersity has been limited to the cylinder core radius. The structural parameters (radius, shell thickness, and polar head groups area) were calculated and are listed in Table 4.

Extracted cylinder lengths are bigger than the maximum accessible dimension and therefore have not been reported. The data suggest that in the micellar state the two surfactants produce similar structures with the same structural parameters within experimental error. These values are consistent with those already obtained from surface tension measurements listed in Table 4.

The packing parameter $p = v_H/(l_H A_p)$, for L-ASC8 and D-ASC8 comes out to be about 0.44, in agreement with the values listed in Table 3 for the different surfactants obtained from the Gibbs equation (eq 2) and is consistent with the formation of cylindrical ($1/3 < p < 1/2$) aggregates.[46] Previous measurements of A_p from surface tension data provided a value for p of 0.36 for L-ASC6, 0.45 for L-ASC14, and 0.49 for L-ASC 16.

Differential Scanning Calorimetry. DSC experiments were performed to determine the transition temperature and enthalpy change for coagel samples as a function of the surfactant concentration (between 5% and 90% w/w). The results (see Figure S11, Supporting Information) indicate that the transition temperature is nearly constant up to 50% and then increases almost linearly. Instead, ΔH is proportional to the surfactant concentration. Comparing these data to those already determined for L-ASCn in the same conditions,[6,47] it emerges that the D-epimers possess slightly lower transition temperatures than the corresponding L-derivatives, whereas the ΔH values are higher (except for D-ASC8).

TABLE 5: Values of ΔH_{hg}, Obtained from Equation 6, and of ΔS_{hg}

	ΔH_{hg} (±10%) (in kJ/mol$_{surf}$)		ΔS_{hg} (±10%) (in J/K·mol$_{surf}$)	
n	D	L	D	L
8	7.5	6.8	21.5	39.6
10	9.8	7.9	6.5	33.8
12	−1.2	−4.2	1.9	5.3

The coagel transition involves different steps:[6,42]

(i) The headgroups separate from their counterions (H^+ in the present case) and heat is taken up (ΔH_{el}).

(ii) Hydration of the headgroups by the surrounding solvent molecules occurs, and heat is released (ΔH_{hydr}).

(iii) Finally, heat is absorbed due to a conformational/packing change of the hydrophobic aliphatic chains (ΔH_{chain}).

In this simplified scheme the first two enthalpic contributions are related to surfactant headgroup−water interactions ($\Delta H_{el} + \Delta H_{hydr}$), and the third is ascribed to the conformational change of the alkyl hydrophobic portion only. The electrostatic (ΔH_{el}) and the conformational (ΔH_{chain}) terms are positive (endothermic processes), whereas the hydration contribution is negative (exothermic process). As the number of carbon atoms in the chain increases, ΔH_{chain} becomes more significant.

For a set of surfactants that share the same headgroup (L-ASCn or D-ASCn), the value of ΔH_{chain} strictly depends on the chain length and will determine the formation of a micellar solution ($n = 8$ or 10) or of a gel (for $n \geq 12$).[42]

It is convenient to separate the contribution related to the headgroups (ΔH_{hg}) from that due to the melting of the aliphatic chains (ΔH_m):

$$\Delta H = \frac{10P}{M}(\Delta H_m + \Delta H_{hg}) \qquad (6)$$

ΔH is measured in J/g$_{sample}$, ΔH_m and ΔH_{hg} are expressed in kJ/mol$_{surfactant}$, and M and P indicate the molecular weight of the surfactant and its concentration (in % w/w) in the sample.

Taking the enthalpy change of melting of the pure surfactants (ΔH_m, see Table 3) as the term that reflects the conformational change of the side chains certainly results in an overestimate of the melting contribution. So the values for ΔH_{hg} (see Table 4) will be underestimated. The values of ΔS_{hg} were calculated in a similar way and are shown in Table 5.

The data suggest that the hydration of the shorter surfactants, which undergo a coagel-to-micelle phase transition, is similar, whereas the values for D-ASC12 and L-ASC12 (that show a coagel-to-gel transition) are presumably due to the different ionization degree of the polar headgroups.[48] Remarkably, the values of ΔH_{hg} for D-ASCn are always larger than those for L-ASCn, confirming the different structural features (bond angles of the $-C_5HOH-C_6H_2OH$ side chain).[29] This result relates the effect of chirality and structural parameters directly to the

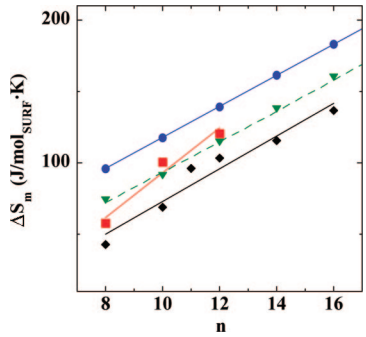

Figure 6. Entropy of melting (ΔS_m) for pure n-alkanes (●), carboxylic acids (▼), L-ASC*n* (◆), and D-ASC*n* (■).

TABLE 6: Area Per Polar Group Values Calculated with Equation 9 for Coagels at 60% w/w of Surfactant

n	D-ASC*n*	L-ASC*n*
8	66	41
10	60	41
12	51	40

thermodynamics of the surfactant nanoassemblies in the condensed state.

Interestingly, although ΔS_m is always larger for the D-derivatives (due to more freedom of lateral motion for the side chain), the value of ΔS_{hg} is always lower for D-ASC*n* with respect to the L-ASC*n* surfactants.

To clarify the significance of the entropic contribution in these systems, we compared the ΔS of melting for pure D-ASC*n*, L-ASC*n*, *n*-alkanes, and carboxylic acids.[42] For a given chain length, the ΔS_m sequence (see Figure 6) is:

$$\text{n-alkane} > \text{carboxylic acid} \geq \text{D-ASC}n > \text{L-ASC}n$$

This reflects the different degree of lateral freedom that the alkyl chains possess in the different compounds in the solid phase. In other words, the trend reflects the different effect of the hydrophilic groups (none in alkanes, −COOH in carboxylic acids, and the ascorbic acid ring in ASC) in anchoring the hydrophobic tails and limiting their lateral motion.

This evidence suggests that in the pure solid state the headgroups in L-ASC*n* compounds are more tightly bound through intermolecular interactions, whereas the D-isoascorbyl heads in D-ASC*n* interact more weakly.

The percentage of strongly bound water in a sample, W_b (%), can be calculated from the decrease of the area of the endothermic peak associated with the melting of bulk water at 0 °C as follows:[49]

$$W_b(\%) = \frac{(333.79 - \Delta H_w)(100 - P)}{333.79} \qquad (7)$$

where ΔH_w is the experimental enthalpy change due to the melting of free water, P is the concentration of the surfactant (in % w/w), and 333.79 J/g is the heat of melting of pure water.[50] The number of strongly bound water molecules per surfactant headgroup (N_b) is given by:

$$N_b = \frac{M_{surf} W_b}{M_w P} \qquad (8)$$

where M_{surf} and M_w are the molecular mass of the surfactant and of water, respectively. For L-ASC*n* we recorded N_b values

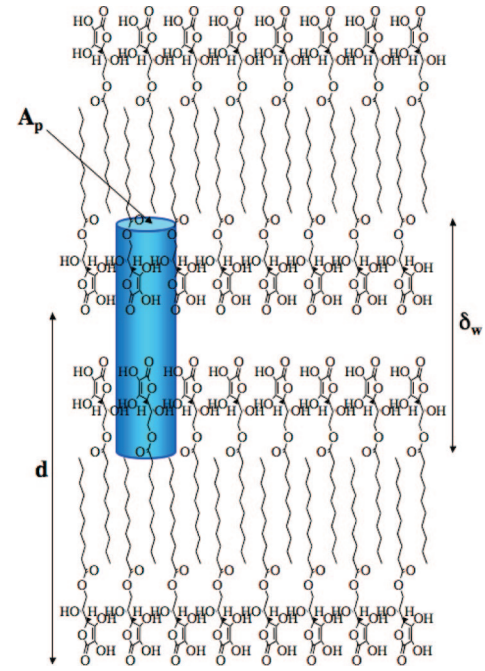

Figure 7. Schematic picture of the coagel microstructure. The surfactant monomers are closely packed in an interdigitated monolayer, with a very small interlayer of strongly bound water molecules. The cylindrical volume element contains two headgroups and their hydration water molecules. d is the spacing obtained from XRD profiles (lowest Bragg angle), δ_w is the sum of the hydration interlayer and two heads, and A_p is the cross-section area per surfactant.

of about 7−25 molecules of water bound to the polar heads, with a slightly higher hydration for the shorter surfactants.[7] Instead, in the case of the D-ASC8 and D-ASC10 (both of which produce micelles after the collapse of the coagel lamellar structure upon heating) we obtain a much larger values of N_b below 30% w/w, between 30 and 150 molecules of water per surfactant. The behaviors of L-ASC*n* and D-ASC*n* are similar when the surfactant concentration is greater than about 50% (see Figure S12, Supporting Information).

We remark here that there is an alternative explanation for such a large number of apparently strongly bound water molecules in D-ASC*n* coagels. As already mentioned, D-isoascorbic acid perturbs the dynamical structure of bulk water strongly.[30,31] Therefore, we can expect that the amount of nonmelting water that we measure indirectly (through DSC at 0 °C) comprises the strongly bound molecules and an undefined amount of "perturbed" water that cannot be considered as hydration water, but whose structure has been destroyed by the D-headgroups in such a way that it does not appear in the melting transition at 0 °C. This point requires further analysis.

SAXS and WAXD. SAXS and WAXD experiments were performed on coagels containing 40% w/w of D-ASC*n* surfactants (see Figures S13 and S14, Supporting Information). The results are listed in Table 6 and are compared to those obtained for L-ASC*n* in the same conditions.

Plotting d versus n and l_H provides values for the slopes $\partial d/\partial n$ and $\partial d/\partial l_H$ that are consistent with interdigitated lamellar monolayers, as for the pure solids.

Figure 7 depicts the tight lamellar microstructure in the coagel phase. The blue cylinder includes two heads and the strongly bound water molecules. If d and $\delta_w = d - l_H$ represent respectively the repeat spacing distance (from SAXS profiles for the hydrated samples), the length of the hydrophilic region (i.e., the height of the cylinder), then the area per polar group in the coagel can be estimated as:

$$2\upsilon_w N_b + 2\upsilon_p = A_p\delta_w \quad (9)$$

where υ_w, N_b, and υ_p are the volume of a water molecule, the number of strongly bound water molecules per polar group, and the volume of a single headgroup.[7] The values of A_p are shown in Table 6. For L-ASC*n* the results are very close to those obtained for the micellar state (see Table 3). This finding indicates that the space occupied by the hydrophilic layer remains almost the same in the micellar and in the coagel states, whereas the different packing and interactions in the hydrophobic core determine the phase behavior of these surfactants. Instead, the value of A_p for the D-ASC*n* amphiphiles in the coagel are larger than those obtained from the Gibbs adsorption equation. However, it must be observed that the value of υ_p for D-isoascorbic acid is certainly smaller than that for L-ascorbic acid (about 275.3 Å^3),[7] and therefore the calculation of A_p values is an overestimate.

In the case of coagels produced by octadecyltrimethylammonium chloride, Kodama and Seki found that for samples with a total water content below 17% w/w, all water exists as nonfreezable, strongly bound interlayer water.[42] Furthermore, they concluded that different crystals are present in the samples, with different degrees of hydration.

Hydration of the headgroups can be treated as an uptake by adsorption of solvent molecules on the lamellar surface and by swelling due to the formation of aqueous cluster in a supramolecular structure.[51,52] Moreover, the hydration of specific polar residues results in a distribution of adsorption energies.

Most likely, a similar situation can be envisaged with the ASC*n* surfactants in the hydrated lamellar phase. Some water molecules strongly interact with the hydroxyl groups of the heads, and more solvent molecules remain confined in the interlamellar space in the gel phase. Further experiments are currently in progress to elucidate the nature of the water molecules differently associated to these nanostructures in the condensed phase.

Conclusions

Chirality, hydrogen bonding, steric features, hydrophobic and π-π interactions, dispersion forces, and other noncovalent interactions are the forms in which information is conveyed by chemical building blocks such as amino acids, surfactants, nucleotides, and other molecules. The arrangement of these species in supramolecular structures and their biological activity are the most important phenomena in which molecular recognition emerges.

In this paper we have reported a detailed study on chiral surfactant derivatives, where the headgroup is made up by either a L-ascorbic or D-isoascorbic moiety. These two acids are epimeric forms, with a configuration inversion at atom C_5 of the side chain.

Such an apparently small change results in a great difference in their physicochemical properties, in the solid and in the dispersed state. In fact, L-ascorbic acid and its derivatives establish several intermolecular hydrogen bondings with other monomers and with water, while intramolecular interactions dominate the scene in D-isoascorbic acid and its derivatives.

We synthesized 6-O-D-isoascorbyl-octanoate (D-ASC8), decanoate (D-ASC10), and dodecanoate (D-ASC12). We performed MIR, NIR, SAXS, WAXD, XRD, DSC, conductivity and surface tension measurements in order to study the main structural and thermodynamic properties of these surfactants and of their nanoassemblies in water dispersions, and we compared the results to those already acquired for the corresponding L-epimers.

The results indicate that the different configurations of the two headgroups produces a different set of inter- and intramolecular interactions that largely affect the thermodynamics of self-assembly greatly and particularly through hydration. D-ASC*n* are less hydrated than L-ASC*n* but probably perturb the dynamic structure of bulk water more efficiently than L-ASC*n*. This finding parallels previous reports that indicate that water structure modification is the main reason for the different biological activity of L-ascorbic and D-isoascorbic acid.

Acknowledgment. The authors acknowledge the Consorzio Interuniversitario per lo Sviluppo dei Sistemi a Grande Interfase (CSGI, Florence) and the Ministero dell'Istruzione, dell'Università e della Ricerca (MIUR, Rome) for partial financial support.

Supporting Information Available: NIR, MIR, XRD, conductivity, surface tension, SAXS, WAXD, phase diagram, and strongly bound water data for L-ASC*n* and D-ASC*n*. This information is available free of charge via the Internet at http://pubs.acs.org.

References and Notes

(1) Capuzzi, G.; Lo Nostro, P.; Kulkarni, K.; Fernandez, J. E. *Langmuir* **1996**, *12*, 3957–3963.
(2) Lo Nostro, P.; Capuzzi, G.; Pinelli, P.; Mulinacci, N.; Romani, A.; Vincieri, F. F. *Coll. Surf. A* **2000**, *167*, 83–93.
(3) Capuzzi, G.; Kulkarni, K.; Fernandez, J. E.; Vincieri, F. F.; Lo Nostro, P. *J. Colloid Interface Sci.* **1997**, *186*, 271–279.
(4) Capuzzi, G.; Lo Nostro, P.; Kulkarni, K.; Fernandez, J. E.; Vincieri, F. F. *Langmuir* **1996**, *12*, 5413–5418.
(5) Palma, S.; Manzo, R.; Lo Nostro, P.; Allemandi, D *Int. J. Pharm.* **2007**, *345*, 26–34.
(6) Palma, S.; Manzo, R. H.; Allemandi, D.; Fratoni, L.; Lo Nostro, P. *Langmuir* **2002**, *18*, 9219–9224.
(7) Ambrosi, M.; Lo Nostro, P.; Fratoni, L.; Dei, L.; Ninham, B. W.; Palma, S.; Manzo, R. H.; Allemandi, D.; Baglioni, P. *Phys. Chem. Chem. Phys.* **2004**, *6*, 1401–1407.
(8) Shalmashi, A.; Eliassi, A. *J. Chem. Eng. Data* **2008**, *53*, 1332–1334.
(9) Esselen, W. B.; Powers, J. J.; Woodward, R. *Ind. Eng. Chem.* **1945**, *37*, 295–299.
(10) Leffingwell, J. C. *Vitamin C (Ascorbic acid) In Chirality & Bioactivity 1*, Pharmacology; Leffingwell Reports: Canton, GA, 2003; pp 8−10.
(11) Hvoslef, J. *Acta Cryst. B* **1969**, *25*, 2214–2223.
(12) Boyd, B. J.; Krodkiewska, I.; Drummond, C. J.; Grieser, F. *Langmuir* **2002**, *18*, 597–601.
(13) Bombelli, C.; Bernardini, C.; Elemento, G.; Mancini, G.; Sorrenti, A.; Villani, C. *J. Am. Chem. Soc.* **2008**, *130*, 2732–2733.
(14) Cornelissen, J. J. L. M.; Rowan, A. E.; Nolte, R. J. M.; Sommerdijk, N. A. J. M. *Chem. Rev.* **2001**, *101*, 4039–4070.
(15) Terech, P.; Weiss, R. G. *Chem. Rev.* **1997**, *97*, 3133–3160.
(16) Ambrosi, M.; Fratini, E.; Alfredsson, V.; Ninham, B. W.; Giorgi, R.; Lo Nostro, P.; Baglioni, P. *J. Am. Chem. Soc.* **2006**, *128*, 7209–7214.
(17) Lo Nostro, P.; Capuzzi, G.; Romani, A.; Mulinacci, N. *Langmuir* **2000**, *16*, 1744–1750.
(18) Palma, S.; Manzo, R. H.; Allemandi, D.; Fratoni, L.; Lo Nostro, P *J. Pharm. Sci.* **2002**, *91*, 1810–1816.
(19) Tanford, C. *J. Phys. Chem.* **1972**, *76*, 3020–3024.
(20) Blanton, T.; Huang, T. C.; Toraya, H.; Hubbard, C. R.; Robie, S. B.; Louer, D.; Gobel, H. E.; Will, G.; Gilles, R.; Raftery, T. *Powder Diffr.* **1995**, *10*, 91–95.
(21) Lake, J. A. *Acta Crystallogr.* **1967**, *23*, 191–194.
(22) Liu, H.; Xiang, B.; Qu, L. *J. Mol. Struct.* **2006**, *794*, 12–17.
(23) Kröger-Ohlsen, M.; Skibsted, L. H. *J. Agric. Food Chem.* **1997**, *45*, 668–676.
(24) Hvoslef, J. *Acta Cryst. B* **1968**, *24*, 1431–1440.
(25) Hvoslef, J. *Acta Cryst. B* **1968**, *24*, 23–35.
(26) Kim, M. S.; Lee, S. H.; Chung, U. T.; Kang, Y. K. *Bull. Kor. Chem. Soc.* **1991**, *12*, 143–148.
(27) Shin, Y. A.; Kang, Y. K. *Bull. Kor. Chem. Soc.* **1991**, *12*, 61–67.
(28) Migliardo, F.; Branca, C.; Faraone, A.; Magazù, S.; Migliardo, P. *Phys. B* **2001**, *301*, 138–140.

(29) Azarnia, N.; Berman, H. M.; Rosenstein, R. D. *Acta Cryst. B* **1971**, *27*, 2157–2161.
(30) Wang, Y.; Tominaga, Y. *J. Chem. Phys.* **1996**, *104*, 1–6.
(31) Umehara, T.; Tominaga, Y.; Hikida, A.; Mashimo, S. *J. Chem. Phys.* **1995**, *102*, 9474–9479.
(32) Mashimo, S.; Miura, N.; Umehara, T. *J. Chem. Phys.* **1992**, *97*, 6759–6765.
(33) Wang, Y.; Tominaga, Y. *J. Phys. Soc. Jpn.* **1993**, *62*, 4198–4201.
(34) *The Merck Index*, 13th ed.; Merck & Co., Inc.: Whitehouse Station, New Jersey, 2001.
(35) Mora, M. A.; Melendez, F. J. *J. Mol. Struct. (Theochem)* **1998**, *454*, 175–185.
(36) Davies, M. B.; Austin, J.; Partridge, D. A.; *Vitamin C: Its Chemistry and Biochemistry*; Royal Society of Chemistry: Cambridge, 1991; pp 36−41.
(37) Lohmann, W.; Pagel, D.; Penka, V *Eur. J. Biochem.* **1984**, *138*, 479–480.
(38) Signorell, R.; Kunzmann, M. K.; Suhm, M. A. *Chem. Phys. Lett.* **2000**, *329*, 52–60.
(39) Tork, A.; Bazuin, C. G. *Macromolecules* **2001**, *34*, 7699–7706.
(40) Ren, B.; Cheng, Z.; Tong, Z.; Liu, X.; Wang, C.; Zeng, F. *Macromolecules* **2006**, *39*, 6552–6557.
(41) Kricheldorf, H. R.; Probst, N.; Schwarz, G.; Wutz, C. *Macromolecules* **1996**, *29*, 4234–4240.
(42) Kodama, M.; Seki, S. *Adv. Colloid Interface Sci.* **1991**, *35*, 1–30.
(43) Kanicky, J. R.; Shah, D. O. *Langmuir* **2003**, *19*, 2034–2038.
(44) Guinier, A.; Fournet, G. *Small-Angle Scattering of X-Rays*; John Wiley and Sons: New York, 1955.
(45) Kline, S. R. *J. Appl. Crystallogr.* **2006**, *39*, 895–900.
(46) Israelachvili, J. N.; Mitchell, D. J.; Ninham, B. W. *J. Chem. Soc., Faraday Trans. 2* **1976**, *72*, 1525–1568.
(47) Lo Nostro, P.; Ninham, B. W.; Fratoni, L.; Palma, S.; Manzo, R. H.; Allemandi, D.; Baglioni, P. *Langmuir* **2003**, *19*, 3222–3228.
(48) Lo Nostro, P.; Ninham, B. W.; Ambrosi, M.; Fratoni, L.; Palma, S.; Allemandi, D.; Baglioni, P. *Langmuir* **2003**, *19*, 9583–9591.
(49) Shikubawa, M.; Aoyagi, K.; Sakamoto, R.; Oguma, K. *J. Chromatogr. A* **1999**, *832*, 17–27.
(50) Dean, J. A. *Lange's Handbook of Chemistry*; McGraw-Hill: New York, 1985.
(51) Benczédi, D.; Tomka, I.; Escher, F. *Macromolecules* **1998**, *31*, 3062–3074.
(52) Blackburn, R. S.; Harvey, A.; Kettle, L. L.; Manian, A. P.; Payne, J. D.; Russell, S. J. *J. Phys. Chem. B* **2007**, *111*, 8775–8784.

JP8092644